Ultrafast energy flow in model biological membranes

Smits, M.; Ghosh, A.; Bredenbeck, J.; Yamamoto, S.; Müller, M.; Bonn, M.

DOI
10.1088/1367-2630/9/10/390
Publication date
2007
Document Version
Final published version
Published in
New Journal of Physics

New Journal of Physics
The open-access journal for physics

Ultrafast energy flow in model biological membranes

Marc Smits[1], Avishek Ghosh[1,2], Jens Bredenbeck[1], Susumu Yamamoto[3], Michiel Müller[4] and Mischa Bonn[1,2,5]

[1] FOM Institute for Atomic and Molecular Physics, Kruislaan 407, 1098 SJ, Amsterdam, The Netherlands

[2] Leiden Institute of Chemistry, Leiden University, PO Box 9502, 2300 RA Leiden, The Netherlands

[3] Stanford Synchrotron Radiation Laboratory, 2575 Sand Hill Road, Menlo Park, CA 94025, USA

[4] Swammerdam Institute for Life Sciences, University of Amsterdam, PO Box 94062, 1090 GB Amsterdam, The Netherlands

E-mail: bonn@amolf.nl

New Journal of Physics **9** (2007) 390
Received 14 May 2007
Published 31 October 2007
Online at http://www.njp.org/
doi:10.1088/1367-2630/9/10/390

Abstract. We report on the energy flow dynamics in model membranes, investigated by surface-specific time-resolved (femtosecond) sum frequency generation spectroscopy. This recently developed technique allows us to probe energy dynamics selectively at the water/lipid interface. We report vibrational relaxation dynamics of C–H stretch modes in the lipid alkyl chains, and reveal that incoherent energy transfer occurs from the excited CH_2 groups to the terminal CH_3 groups. We also find evidence for strong anharmonic coupling between different CH_2 and CH_3 modes. Relaxation and the energy transfer processes within the lipid alkyl chain occur on (sub-)picosecond timescales. Studies of the dynamics on different lipid phases (gel or liquid crystalline phase) reveal a marked independence of the dynamics on the precise molecular conformation of the lipids. In addition, we report the energy transfer dynamics between membrane-bound water and lipids, and find that the transfer of heat between water and lipids occurs remarkably fast: heat is transferred across the monolayer, from the polar head group region of the lipid to the end of the alkyl chain, within 1 ps. These results demonstrate the potential of using ultrafast surface-specific spectroscopies to elucidate biomolecular dynamics at membrane surfaces.

[5] Author to whom any correspondence should be addressed.

PII: S1367-2630(07)50412-X

Contents

1. Introduction

The dynamics of excitation transfer and energy flow in biological systems have been studied extensively in the past decade [1, 2], for several reasons. First of all, a number of important biological processes rely on fast energy transfer processes. In photosynthesis, for example, the events that occur when photons impinge on a light harvesting complex, involve the excitation going through several intermediate states before reaching the reaction center; the initial steps in this energy migration process occur on femtosecond timescales [3]. It is evident that a complete understanding of photosynthesis requires insights on all relevant timescales.

Moreover, it has become apparent that even for biofunctionality that does not rely on large-scale, dynamical energy transfer processes, dynamical studies can provide important insights into biomolecular processes and functions: it is becoming increasingly clear that insights into the static structure of biomolecules is not always sufficient to completely understand their function [4, 5]. For instance, conformational fluctuations that may occur over many timescales have been shown to play an important role in protein action [4], [6]–[8].

This realization is prompting increasing efforts to elucidate dynamical aspects of biomolecular structure and functioning. Indeed, femtosecond, time-resolved studies of biomolecules which probe the energy dynamics in biomolecules is providing important information about the function of those biomolecules, which cannot be obtained from static experiments [7]–[11]. Although biomolecular dynamics are being studied extensively in bulk biological systems (see e.g. [1, 2], [7]–[12] and references therein), this is less so for biological surfaces, most notably membranes [11], [13]–[16]. This is remarkable, considering that up to 40% of all cellular proteins—the micro-machines of life—are embedded in membranes. Our understanding of this intricate surface is essential to comprehend—and ultimately control—the many biochemical and biomedical processes that occur at, or even within, the membrane surface, including viral infection and targeted drug delivery. The reason for this lag in our

knowledge is therefore clearly not the lack of relevant questions, but the limited number of techniques that are sufficiently sensitive and surface specific to probe molecular dynamics (MD) in a membrane. Indeed, much of our knowledge of membrane protein and lipid dynamics originates from molecular dynamics MD simulations (see, e.g. [17]).

The reports mentioned above [1, 2], [7]–[12], [16] are based on femtosecond laser spectroscopy. This approach is uniquely suited to provide direct access to biomolecular dynamics, by investigating the temporal evolution of the biomolecular system in real-time. As such, the approach complements techniques that infer biomolecular dynamics in membrane systems from steady-state measurements, such as time-domain fluorescence (upconversion [18] or correlation [19]) spectroscopies, electron spin resonance/electron paramagnetic resonance (ESR/EPR) [20, 21] and NMR (see e.g. [22, 23] studies of membrane dynamics, neutron [24, 25] and x-ray scattering [26, 27]).

Indeed, there have been several femtosecond laser-based studies addressing the dynamics of biological membrane model systems, notably water–lipid interactions [13]–[15] and transmembrane proteins [11, 16]. We present here the first surface-specific study of vibrational energy relaxation and energy transfer in such a model membrane system. The technique presented here—time-resolved sum frequency generation (TR-SFG)—has the advantage of being surface specific. The experiments reported here were performed on lipid monolayers prepared on an ultrapure water subphase, which allows for detailed control of the membrane parameters, e.g. the surface pressure and lipid phase.

Our method relies on exciting specific vibrational modes within, or at, the membrane surface and monitoring the subsequent energy relaxation and transfer processes with femtosecond time resolution. The cell membrane consists of two leaflets of lipids where the hydrophobic chains of the lipid form the interior of the membrane and the hydrophilic headgroups face the aqueous environment [28]. Our model membrane is a self-assembled lipid monolayer on water. Monolayers are considered excellent model systems for membrane biophysics, since a biological membrane can be considered as two weakly coupled monolayers [29]. We study monolayer vibrational dynamics using the surface-specific vibrational spectroscopy of second-order nonlinear sum frequency generation (SFG) spectroscopy [30]–[32]. A limited number of time-resolved studies of specifically surface properties have been reported [33]–[41], but this is, to the best of our knowledge, the first application of this technique to lipid systems.

Lipid layers can be in different thermodynamic phases, depending on lipid composition, temperature and lateral pressure [42]. Different lipid phases exhibit different properties, e.g. in terms of the mobility of constituents. Thus, the phase behavior of lipids is very important for the functioning of a membrane. Owing to its relevance, the study of (model) membrane phase behavior has therefore received much attention [43]. Fluorescence studies (e.g. [44]–[46]) have revealed domain formation in biological and model systems, and have provided important information about the mobility of membrane components, i.e. membrane fluidity. The lipid phase can be traced directly to the order/disorder state of the lipid hydrocarbon chain. For a highly compressed, saturated lipid, the alkyl chain will be in an ordered all-trans configuration (figure 3). Lipids with a lower degree of saturation may be in the more fluid crystalline liquid state at room temperature. This state is characterized by gauche defects in the alkyl chain, to which SFG is extremely sensitive.

Indeed, steady-state SFG spectroscopy has been applied extensively to study lipid and surfactant interfaces [47]–[51]. This paper reports the first TR-SFG measurements of the energy

flow in model membranes. We report on the vibrational relaxation of the C–H modes in lipids in different thermodynamic phases (the ordered gel and disordered liquid crystalline phase), as well as the dynamics of energy transfer between the water and the lipid.

The outline of the paper is as follows: first, the basic principles of the surface specific SFG technique are discussed in section 2. Here, it is also explained how an infrared (IR) pump field can be added to the SFG scheme to measure the dynamics of vibrational energy relaxation and energy transfer processes. In section 3, schematics of the experiment, the detection technique and sample preparation methods are provided. The results for the measurements of the vibrational relaxation and energy transfer are presented in section 4, as well as the analysis to obtain the lifetimes and transfer rates from the experimental data. Finally, the findings are compared to previous bulk studies in section 5, which reveals the specifics of the role of the interface in the relaxation dynamics.

2. Time-resolved surface spectroscopy

Our experimental approach relies on pump–probe spectroscopy. An ultrashort (femtosecond) IR pump pulse excites a specific vibration within the model membrane (e.g. a C–H stretch vibration within the lipid alkyl chain or the O–H stretch vibration of membrane-bound water). The relaxation and energy transfer dynamics are interrogated by a second, delayed probe pulse pair, using femtosecond TR-SFG spectroscopy. This technique provides direct, non-invasive access to membrane lipids and membrane-bound water, through their molecular vibrations. TR-SFG relies on the resonant enhancement of frequency mixing when an IR pulse is resonant with a surface vibration. It is inherently surface sensitive (owing to broken inversion symmetry at the surface [30]), and therefore only probes $\sim$1 monolayer deep. The time resolution is determined by the duration of the laser pulses ($\sim$120 fs); the time delay between the excitation and probing pulses can be varied in a controlled manner by increasing the optical path length traveled by the probe pulses. As the laser probes an area of typically $\sim$0.1 mm^2, it interacts with a large number of molecules (typically $\sim 10^{11}$). Molecular scale information is obtained through the molecular vibrations, and the synchronized response of the individual molecules in the membrane ensemble following the excitation process.

Before discussing the time resolved technique in detail, the main features of the SFG probe are briefly discussed first. Subsequently, the technique of TR-SFG is detailed, in particular the similarities and differences to common time resolved techniques like transient IR spectroscopy.

2.1. Steady-state SFG

In the TR-SFG scheme presented here, the second-order nonlinear technique of SFG is applied as a probe. As illustrated in figure 1, SFG relies on the resonant enhancement of the process of generating the sum frequency of an IR and a visible (VIS) photon when the former is resonant with a vibrational transition. This process is governed by the second-order nonlinear susceptibility $\chi^{(2)}$ of the system. Due to symmetry considerations, $\chi^{(2)}$ vanishes in isotropic, centro-symmetric bulk media, such as water. At the interface, the symmetry is necessarily broken and second-order nonlinear processes are allowed.

In the experiment, an IR and a VIS laser beam are spatially and temporally overlapped at the surface, inducing a nonlinear polarization at a frequency which is the sum of the frequencies of the two incoming fields: $\omega_{\mathrm{SFG}} = \omega_{\mathrm{IR}} + \omega_{\mathrm{VIS}}$. In figure 1, a schematic representation of the

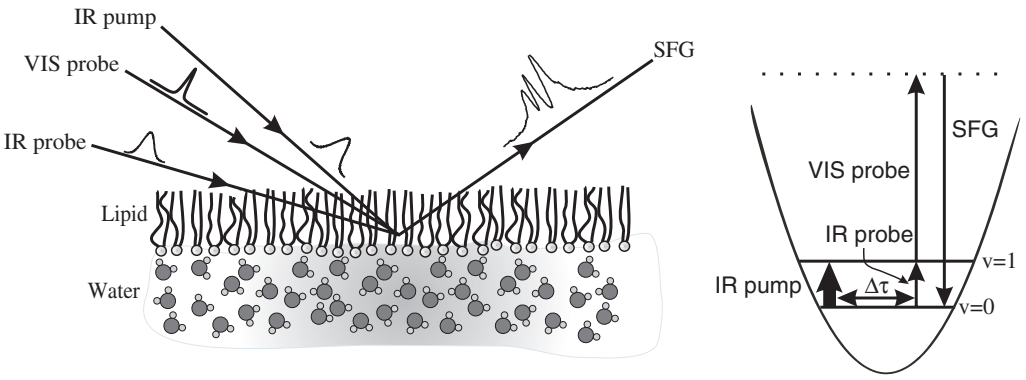

Figure 1. The experimental geometry of TR-SFG spectroscopy is shown in the left panel for a water–lipid interface. The IR probe and VIS probe are overlapped in space and time at the surface to generate an SFG signal. In a TR-SFG experiment, an additional IR pump beam is overlapped with the probe beams, which induces a change in the SFG signal. In the right panel, an energy diagram of the TR-SFG scheme is presented. The IR pump field transfers population from the ground ($v = 0$) to the first excited vibrational level ($v = 1$), decreasing the SFG signal. Vibrational relaxation will repopulate the ground state and the original SFG signal will be recovered. SFG generated from the IR pump and VIS probe can be spatially filtered out.

water–lipid interface is shown with the IR and VIS probe beams (the pump IR beam will be discussed later). The generated SFG signal is emitted both in transmission (not shown) and reflection, conserving the phase-matching of the in-plane components of the wavevectors. The SFG intensity I_{SFG} is proportional to the nonlinear Fresnel factors L [52], the nonlinear susceptibility tensor $\chi^{(2)}$ and the intensities of the incoming fields I_{VIS} and I_{IR}:

$$I_{\mathrm{SFG}} = L \left|\chi^{(2)}\right|^2 I_{\mathrm{VIS}} I_{\mathrm{IR}}. \tag{1}$$

For a nonresonant VIS and SFG field, the nonlinear susceptibility tensor can be described as:

$$\chi^{(2)} = A_{\mathrm{NR}} \exp(\mathrm{i}\phi) + \sum_n \frac{A_n (N_{0,n} - N_{1,n})}{\omega_{\mathrm{IR}} - \omega_n + \mathrm{i}\Gamma_n}. \tag{2}$$

Here, the vibrational resonance n is characterized by amplitude A_n, frequency ω_n and width Γ_n. A relatively small amount of SFG can also be generated away from the resonance; this process is characterized by A_{NR} and ϕ representing the nonresonant amplitude and phase. The resonant amplitude A_n depends on the population difference between the excited and ground states $\Delta n = N_{0,n} - N_{1,n}$. The probe IR field is sufficiently weak that Δn remains unchanged; at room temperature $\Delta n/(N_{0,n} + N_{1,n})$ is close to unity for high-frequency vibrations, such as the C–H and O–H stretch. When the IR field is resonant with a vibrational transition, the SFG signal is enhanced and a vibrational spectrum of surface molecules is obtained.

Femtosecond laser pulses inherently support a large bandwidth ($\sim$200 cm^{-1}, in our case). We therefore make use of a multiplex SFG scheme as described elsewhere [53]–[55]. Using a broadband IR field several spectrally narrow vibrations can be addressed resonantly at once, and a full spectrum is recorded without the necessity of tuning the IR wavelength. The spectral resolution is governed by the narrowband ($\sim$10 cm^{-1}) VIS upconversion field.

2.2. TR-SFG

As shown in equation (2), the effective nonlinear susceptibility tensor is proportional to the population difference between the first excited and the ground state: $\chi^{(2)} \sim \Delta n$. In the TR-SFG scheme, a vibrational transition is excited with a resonant IR pump, changing Δn and the subsequent relaxation dynamics (the decay back from the vibrationally excited state $v = 1$ to the vibrational ground state $v = 0$) can be followed by probing the nonlinear susceptibility after a variable delay time τ using the SFG probe pair. The geometry of the different beams is depicted in figure 1, and the energy-level diagram of the technique is shown in the right panel. Due to the pump-induced population transfer from the ground to the excited state, the population difference Δn becomes smaller temporarily, and the SFG signal decreases accordingly. In other words, after the arrival of the pump pulse, a transient decrease of the signal ('bleach') is observed. The population distribution will subsequently evolve back to equilibrium by vibrational relaxation and the original SFG level will be recovered. This technique has been implemented previously in the picosecond regime [33]–[37], [40]. Recently this technique has been applied with femtosecond time resolution, so far only to probe adsorbates on metal surfaces [41] and interfacial water [38, 39].

A full quantitative expression for the TR-SFG signal can be derived using time dependent perturbation theory [34]. Here, we employ a simplified version of that approach based on the steady-state description. It neglects the finite vibrational coherence time and the coherent interactions between the pump and probe IR fields, therefore introducing a demonstrably small (a comparison of experimental results with IR pump and IR probe polarized parallel and perpendicular reveals that coherent coupling effects are negligible) error around time zero. The simplified approach also implicitly assumes that higher vibrational states do not contribute to the signal. In addition to the effects mentioned below that serve to reduce the intensity of the $v = 2 \leftarrow 1$ transition, the anharmonicity of the C–H is sufficiently large (50–100 cm^{-1}) [56, 57] that it does not interfere with the (modulation of the) fundamental SFG signal.

The fourth-order signal is described using an effective (time-dependent) second-order nonlinear susceptibility tensor. The time dependence of the tensor is contained in the population densities in the ground (N_0) and excited state (N_1), so that:

$$I_{\mathrm{SFG}} \propto \left(A_n(N_{0,n} - N_{1,n})\right)^2 \propto \left(N_{0,n} - N_{1,n}\right)^2. \tag{3}$$

The TR-SFG approach resembles the more widely-applied technique of transient IR spectroscopy, where a pump pulse transfers population to a vibrationally excited state, and a probe pulse directly interrogates the population dynamics. This means that a third-order coherence is being detected (two interactions with the pump and one interaction with the probe) [58]. In the TR-SFG scheme presented here, the main difference is that the third-order coherence is upconverted with the VIS field to a fourth-order coherence. As a result, the observed bleach of the signal is proportional to the square of the population difference, rather than simply the difference [59]. This has some interesting consequences: for example, when the pump excites 10% of the ground state molecules to the excited state, the population difference amounts to $\Delta n = 0.9 - 0.1 = 0.8$. The signal level thus decreases to $\Delta n^2 = 0.8^2 = 0.64$ and a bleach of 36% is observed. Note, however, that the bleach is to first-order still linearly proportional to the population density N_1. Using $N_0 + N_1 = 1$ and therefore $N_0 - N_1 = 1 - 2N_1$, the signal can be rewritten as

$$I_{\mathrm{SFG}} \propto (1 - 2N_1)^2 = 1 - 4N_1 + 4N_1^2. \tag{4}$$

As long as the population transfer is small, the N_1^2 term can be neglected and the signal is linearly dependent on N_1.

To facilitate a direct comparison with transient IR measurements, the normalized TR-SFG signals $\sqrt{S'}$ may be expressed as:

$$\sqrt{S'} = \sqrt{\frac{S(\tau)}{S_0}}, \tag{5}$$

where $S(\tau)$ represents the SFG intensity at pump delay τ, and S_0 the reference signal with the pump field off. Note, however, that a few differences with e.g. transient IR experiments remain: (i) most importantly, SFG selectively probes the surface and hence provides a method to study the dynamics of specifically interfacial molecules (note that, although the probing process is surface specific, the IR pump excitation is not and both surface and bulk molecules will be excited); (ii) SFG from the $v = 2 \leftarrow 1$ transition (the analogy of a pump-induced absorption, also known as hot band), redshifted by the self-anharmonicity of the vibration, is very weak. For the same example of 10% excitation transfer, corresponding to a bleach of 36%, the excited state SFG signal is proportional to $(N_1 - N_2)^2 = 0.1^2 = 0.01$. With an excited state nonlinear susceptibility that is a factor two larger than the ground state susceptibility, the excited state signal is still ~20 times smaller; (iii) in conventional time-resolved IR spectroscopy, when different vibrational resonances are present in the steady-state spectrum, the (transient) spectrum can be described by a linear combination of, e.g. Lorentzian lineshapes. For SFG, the coherent nature of the process dictates that the vibrational resonances can interfere with one another. This means that changes in one resonance due to vibrational excitation will affect the spectral shape of other resonances in the proximity. To correctly infer the dynamics from the transient spectra, it is therefore necessary to fit the peaks of each vibration using equation (2) to obtain the amplitudes A_n for every mode at each delay time. The time-dependent differential TR-SFG signal for a specific amplitude A'_n is therefore computed in terms of the fitted amplitude $A_n(\tau)$ at pump delay τ and the fitted amplitude A_{n0} of the reference with the pump off

$$A'_n = \frac{A_n(\tau)}{A_{n0}}. \tag{6}$$

In our data analysis, we fit the two SFG spectra with pump on and pump off to expressions 2 and 1 for each delay time, varying only the amplitudes A_n between the spectra. The ratio A'_n then provides a direct measure of the temporal evolution of the vibrational population.

3. Experiment

The study of ultrafast surface dynamics with TR-SFG, requires an intense IR pump, an IR probe and narrowband VIS field. The pump-induced decrease in the SFG signal is detected by alternating the pump field on/off, and computing the ratio of the SFG signals. The lipid monolayers were prepared using the Langmuir–Blodgett method on a H_2O or D_2O subphase. Details of the laser set-up and the sample preparation methods are presented below.

3.1. Set-up

For this study, a commercial Ti:Sa femtosecond amplified laser system was used, consisting of an oscillator (Mira, Coherent) and a regenerative/multi-pass amplifier (Titan, Quantronix) with

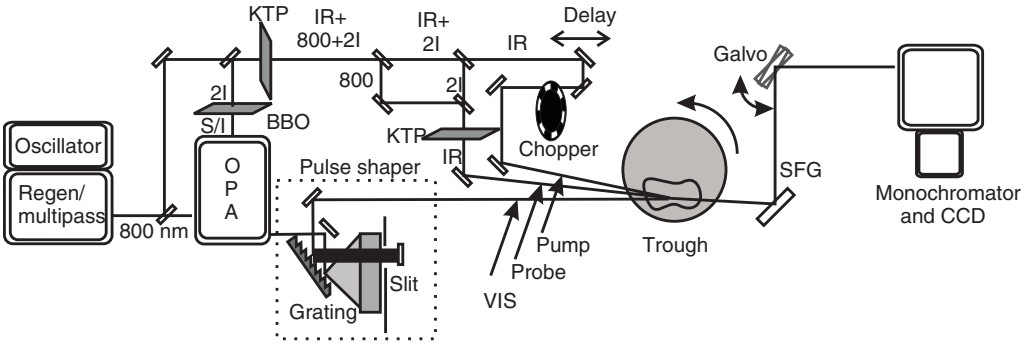

Figure 2. Schematic representation of the experimental set-up. The output of a 1 kHz amplified femtosecond laser system is used to generate IR pump and probe pulses in a two-step process; narrowband VIS pulses are generated in a pulse shaper with an adjustable slit to select the wavelength. The pump IR beam can be variably delayed using an optical delay line, is mechanically chopped to 500 Hz and all beams are intersected at the interface. The SFG generated at the interface from the IR probe and the VIS beams is dispersed by a monochromator and imaged onto a CCD array. On the CCD, the SFG signal with the pump on is displaced vertically with a galvano mirror from the signal with pump off at 500 Hz

pulse characteristics 800 nm/100 fs/1 kHz. To produce sufficient energy for the pump IR field and to have the flexibility of an IR probe field with a different central wavelength, the scheme in figure 2 was used. The IR was generated in a two-step process as detailed elsewhere [60]. Briefly, 1 mJ of the Ti:Sa output was used for an optical parametric generation/amplification (OPG/OPA) (traveling wave optical parametric amplifier (TOPAS) Light Conversion) to produce an idler field centered at a wavelength of 2.2 μm. This field was first frequency doubled in a β barium borate (BBO) crystal and subsequently mixed with 2 mJ of the 800 nm Ti:Sa output to generate the difference frequency in a 3 mm $KTiOPO_4$ (KTP) crystal. In this way, IR pump pulses of $>80\,\mu$J and 120 fs could be produced. Since difference frequency mixing is a parametric amplification process, the amount of doubled idler was increased during the IR generation. It was feasible to split off the amplified doubled idler field and generate again the difference frequency in a second KTP crystal with the residual 800 nm field. Because the doubled idler field was amplified in the mixing process, it was possible to detune the KTP crystal from the central wavelength to the wing of the doubled idler spectrum. With this method it was possible to generate IR pump and probe fields that are separated by $> 200\,\mathrm{cm}^{-1}$ and probe energies of 10 μJ. In the one-color experiments, where the KTP crystal was changed to center wavelength, the probe energy increased to 30 μJ. The narrowband VIS pulse was generated using the residual Ti:Sa 800 nm light out of the TOPAS. A home built pulse shaper was used to select only part of the spectrum with an adjustable slit.

The IR pump, the IR probe and VIS probe beams were focused and intersected at the interface with beam waists of respectively ~150, ~100 and ~100 μm. The IR pump focus is slightly larger in order to probe an area that is homogeneously excited. All beams were in the same vertical plane and made angles with the surface normal of respectively 40°, 50° and 60° for the IR pump, the IR probe and VIS probe beam. The IR pump was scanned in time using a delay line and was mechanically chopped to alternate pump on/off at 500 Hz.

The SFG signal was detected in reflection mode and residual (mainly VIS) light was filtered out with short wave pass filters. The SFG light was spectrally dispersed using a monochromator (Acton 300i) and detected using an intensified charge-coupled device (iCCD) camera (PiMaxIII, Roper Scientific). SFG signals with pump on or off are separated spatially by a galvano mirror (GSM1005, GSI Lumonics). This mirror alternates its position every millisecond to project the signal with the pump on at the top of the CCD array and the signal with the pump off at the bottom. After typically 5 s acquisition time, the complete image was transferred to a PC where the spectra were stored individually.

For a nonresonant VIS field the molecular response to the VIS field is essentially instantaneous and therefore the experimental response time is determined by the IR fields. IR pulse durations of $\sim$120 fs were measured by performing sum-frequency generation of the pump and probe IR fields and the VIS field as a function of delay between IR pump and probe fields.

The polarization of the IR and VIS fields is set with individual $\lambda/2$-plates. The SFG probing process is characterized by a three-letter combination signifying the three polarizations of the SFG, VIS and IR beams, respectively. The experiments presented here were performed in SSP-mode. The polarization of the IR pump field can be chosen to be parallel or orthogonal to the IR probe field. Parallel and perpendicular excitation pulses result in different preferential excitations within the lipid monolayer: the terminal methyl group of the phospholipid chains has its transition dipole of the symmetric CH_3 stretch at an angle of 30° with respect to the surface normal [52]. As a result, when there is no reorientation of the lipid chains after excitation, the expected bleach for the P-polarized pump is expected to be larger than for the S-polarized pump. The symmetric stretch vibration of the CH_2 groups, in contrast, has a predominantly in-plane character, and is therefore most efficiently excited with horizontal (S-)polarized light.

3.2. Sample preparation

The lipids 1,2-dipalmitoyl-sn-glycero-3-phosphocholine (DPPC), 1,2-dioleoyl-sn-glycero-3-phosphocholine (DOPC) and 1,2-dipalmitoyl-3-trimethylammonium-propane (DPTAP) were purchased from Avanti Polar Lipids and were used without further purification. The chemical structures are depicted in figure 3. Solutions of the lipids were made in chloroform. The lipid monolayer was spread using a drop cast method in a home-built Teflon trough while monitoring the surface pressure with a Wilhelmy plate tensiometer (Kibron). All measurements were carried out at surface pressures of $\Pi \approx 25\,\mathrm{mN\,m^{-1}}$, where at room temperature DPPC and DPTAP are in the highly ordered gel phase, but DOPC is in the disordered liquid crystalline phase. Hence, the tails of DPPC and DPTAP are all straight up in a all-trans (zigzag) configuration, whereas in the case of DOPC, the tails are much more randomly oriented and have gauche defects with cis-trans configurations (see cartoons in figure 3). For the subphase, either distilled Millipore filtered H_2O (18 MΩ cm resistivity) of pH 7, or commercially obtained D_2O (Cambridge Isotopes, 99.96% D) was used.

For the temperature dependent measurements of H_2O-DPTAP, the trough was heated or cooled with four Peltier elements from 10° up to 60°. The temperature was measured using a thermocouple. To prevent the formation of bubbles upon heating, the water was degassed prior to the experiment.

To avoid the effect of laser damage of the sample due to repeated laser shots, the trough was rotated to completely refresh the sample every 10 laser shots. New samples were prepared after every 3 h of data acquisition, if necessary.

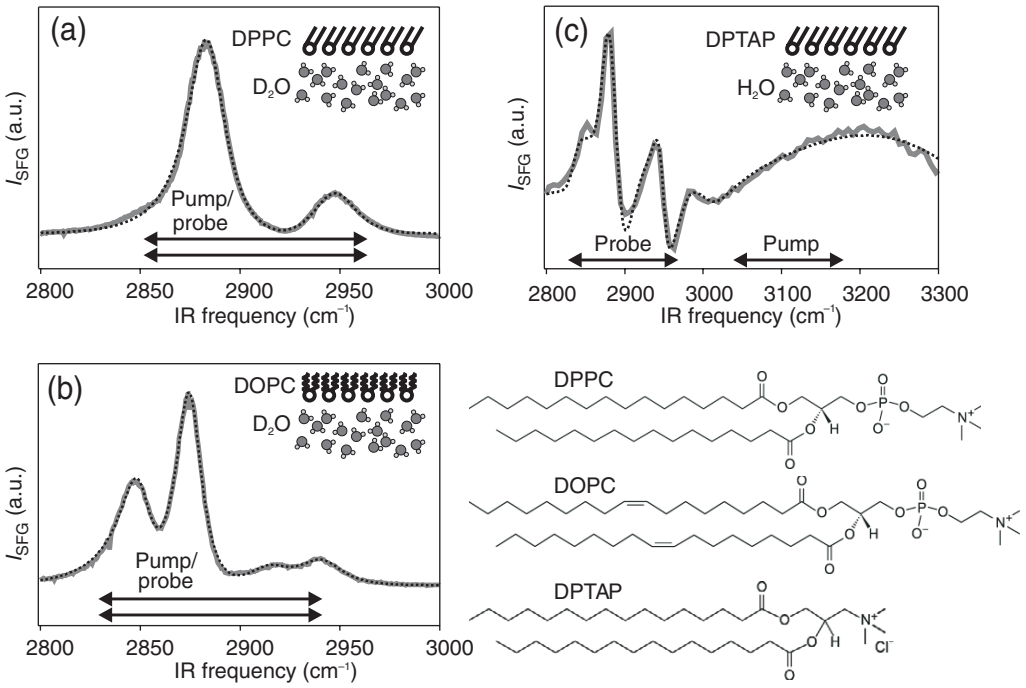

Figure 3. The steady-state SFG spectra (solid gray line) are shown for D_2O-DPPC (a), D_2O-DOPC (b) and H_2O-DPTAP (c) at room temperature and surface pressures of $\Pi \sim 25\,\mathrm{mN\,m^{-1}}$. For DPTAP, additional spectra at 30, 40 and 50°C are shown. The dashed black line is a fit to the experimental data. For the assignment of the peaks, see text. The chemical structures of the lipids are shown for convenience and the phase of the lipids is indicated by the cartoon next to the spectrum.

4. Results

4.1. Steady-state SFG spectra

In figure 3, the steady-state spectra for monolayers of DPPC (a), DOPC (b), both on D_2O and DPTAP on H_2O (c) at room temperature and surface pressures of $\Pi = \sim 25\,\mathrm{mN\,m^{-1}}$ are shown as gray lines in the C–H stretch region from 2800 to 3000 $\mathrm{cm^{-1}}$ (for H_2O-DPTAP up to 3300 $\mathrm{cm^{-1}}$). The spectra are not corrected for the Gaussian shaped IR power spectrum. The spectra for DPPC and DOPC are recorded during the time resolved measurements on a D_2O subphase as the average of all the spectra recorded with the pump field off. The DPTAP on H_2O is recorded in a separate set-up where the IR wavelength was scanned to include the O–H stretch region of water. The spectrum shows the wing of the water spectrum that interferes with the C–H stretch bands. The assignment of the peaks are well-known from literature. All spectra show the CH_3 vibrations: symmetric stretch $\nu_{s,CH3}$ at 2870 $\mathrm{cm^{-1}}$, Fermi resonance ($\nu_{FR,CH3}$) at 2940 $\mathrm{cm^{-1}}$ and antisymmetric stretch vibration $\nu_{as,CH3}$ at 2955 $\mathrm{cm^{-1}}$. For DPPC and DPTAP, the CH_2 resonances are almost invisible, due to the high degree of order within the lipid alkyl chain: in the ordered all-trans configuration, the chain has inversion symmetry and, as a result, the CH_2 resonances are SFG inactive. For DPTAP, a slight CH_2 (at 2847 $\mathrm{cm^{-1}}$) contribution can be observed due to laser heating of the sample. Since DOPC is in the disordered liquid crystalline

phase at room temperature, the alkyl chains have many gauche defects and the CH_2 vibrations are clearly observed: the symmetric CH_2 stretch at 2847 cm^{-1} ($\nu_{s,CH2}$), antisymmetric stretch at 2911 cm^{-1} ($\nu_{as,CH2}$) and Fermi resonance ($\nu_{FR,CH2}$) at 2893 cm^{-1}. For the case of DOPC, where the resolution has to be sufficient to distinguish the CH_2 and CH_3 peaks, the VIS pulse shaper is operated in high-resolution mode at the expense of intensity and signal-to-noise. The dashed black lines in figure 3 are fits of the data using equation (2) and the literature values for the resonance frequencies.

The SFG peak around 2950 cm^{-1} contains contributions from both $\nu_{as,CH3}$ and $\nu_{FR,CH3}$, with a four times larger contribution from the former. In the analysis of the time-resolved spectra, the influence of the much smaller $\nu_{FR,CH3}$ is neglected in this study.

For the dynamical studies, the average spectra of ∼125 000 laser pulses, the IR pump being alternatingly switched on and off, are obtained at typically 40 time points. Next, each of these spectra are fit individually to account for the interference effects as discussed in section 2.2 and to obtain the amplitudes A in equation (2) that are proportional to the population differences between different vibrational levels. And finally, the ratio between the amplitudes with the IR pump on/off as a function of time delay are computed for each vibration. Data is collected up to 100 ps to accurately obtain the final signal level.

4.2. TR-SFG spectra

4.2.1. DPPC. In a first set of experiments, the vibrational relaxation of lipid monolayers was investigated using a one-color experiment with pump and probe IR wavelength centered at ∼ 2900 cm^{-1}. Owing to the large bandwidth of the IR pulses, all CH_2 and CH_3 vibrations in the lipid alkyl chain are excited simultaneously. The relaxation of the different modes can be followed independently using the amplitudes of the different SFG resonances, as explained in section 2.2. A D_2O-subphase was used to avoid the heating of the subphase by the IR pump pulse. Heating by the IR pump pulse is suppressed in D_2O, since the O–D vibrations are far off from the IR pump frequency. The polarizations of the SFG, VIS and probe IR fields were respectively S, S and P.

A typical experimental result is shown in figure 4, which reveals a decrease in SFG intensity for all frequencies within the bandwidth (most evident for the symmetric CH_3 stretch around 2880 cm^{-1}). Fits to the data are also shown, with the individual amplitude for the symmetric CH_3 stretch shown as dotted lines. These amplitudes are used to infer the vibrational dynamics for the different modes.

In figure 5, the time traces for the inferred amplitudes of the susceptibility for the terminal CH_3 vibration are shown as open squares for $\nu_{s,CH3}$ (a) and $\nu_{as,CH3}$ (b) for the parallel pump and probe IR fields (P-polarized). For the orthogonal pump and probe IR field (pump: S-polarized), the data for $\nu_{s,CH3}$ is shown in panel (c) and for $\nu_{as,CH3}$ in panel (d).

The main features are the bleach due to excitation to the first vibrational level and recovery of the signal by vibrational relaxation. It is apparent that relaxation occurs significantly quicker for the $\nu_{as,CH3}$ mode than for the $\nu_{s,CH3}$ mode. The relaxation rates will be quantified in the next section. The bleach for the case of parallel polarized pump and probe IR fields is significantly larger than for the orthogonal case: for $\nu_{s,CH3}$ the bleach is respectively ∼15 and ∼5%, and for $\nu_{as,CH3}$ respectively ∼10 and ∼2%. For the symmetric CH_3 stretch vibration, the transition dipole has an angle of 30° with respect to the surface normal which implies that the bleach for the P-polarized pump is indeed expected to be larger than for the S-polarized pump. The overall

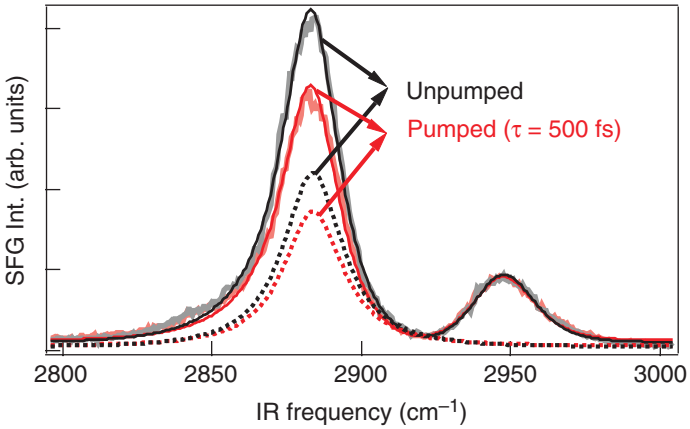

Figure 4. Pumped and unpumped SFG spectra at a pump–probe delay of 500 fs for DPPC. The thin solid lines are fits to the experimental data using models as detailed in section 2; the dotted lines show the fitted amplitudes of the $\nu_{s,CH3}$-mode, which are used to determine the vibrational relaxation time for this mode.

signal-to-noise ratio is better for the symmetric vibration than for the asymmetric, because the SFG intensity is much larger.

In most of the time traces, in particular panel (a) and (c) of figure 5, a decrease of the SFG signal is observed before the pump arrival. This can be explained by the perturbed free induction decay [61]: the probe IR field induces a coherent polarization that decays with the decoherence time constant T_2. As long as this coherent polarization exists and the VIS pulse is present, an SFG signal will be generated. At small negative delay, the pump pulse arrives at the sample after the probe pulse has interacted with the sample, but before the coherent polarization has completely decayed. As a result, the pump can change the signal already at negative delay. This process only affects the data before time $t = 0$ fs, does not affect our conclusions and is not included in the analysis of the data.

Surprisingly, for orthogonal polarizations of pump and probe, the signal is not only smaller (panel (c) of figure 5), but there is clearly a second, much slower, contribution to the bleach of $\nu_{s,CH3}$. This process cannot be attributed to a bleach due to laser excitation, because the FWHM pulse duration of the IR field is $<$120 fs. Since the slow component cannot be attributed to direct laser excitation of $\nu_{s,CH3}$, this process must be caused by energy transfer from a different mode. Because this component is only observed in the data with the pump IR field S-polarized, the energy transfer is most likely from the CH_2 vibrations whose transition dipole moments are parallel to the interface. The pump field excites the in-plane CH_2 vibrations more efficiently when the pump field is polarized parallel to the surface (i.e. S-polarized). The observed energy transfer process from the CH_2- to the CH_3-groups can be of either a coherent, or incoherent nature. In a coherent process, vibrational excitation transfer occurs from the CH_2- to the CH_3-groups: the efficient excitation of the CH_2-groups results in excitation of the CH_3-groups, in addition to direct excitation of the CH_3-groups by the pump pulse. The observed energy transfer process can, however, also be due to incoherent processes: if the CH_2-groups relax quickly, this will result in a very fast local increase in temperature within the lipid monolayer, which may affect the CH_3 signal. It will be shown below that we have strong indications that the latter, incoherent process is responsible for the delayed signal in-growth.

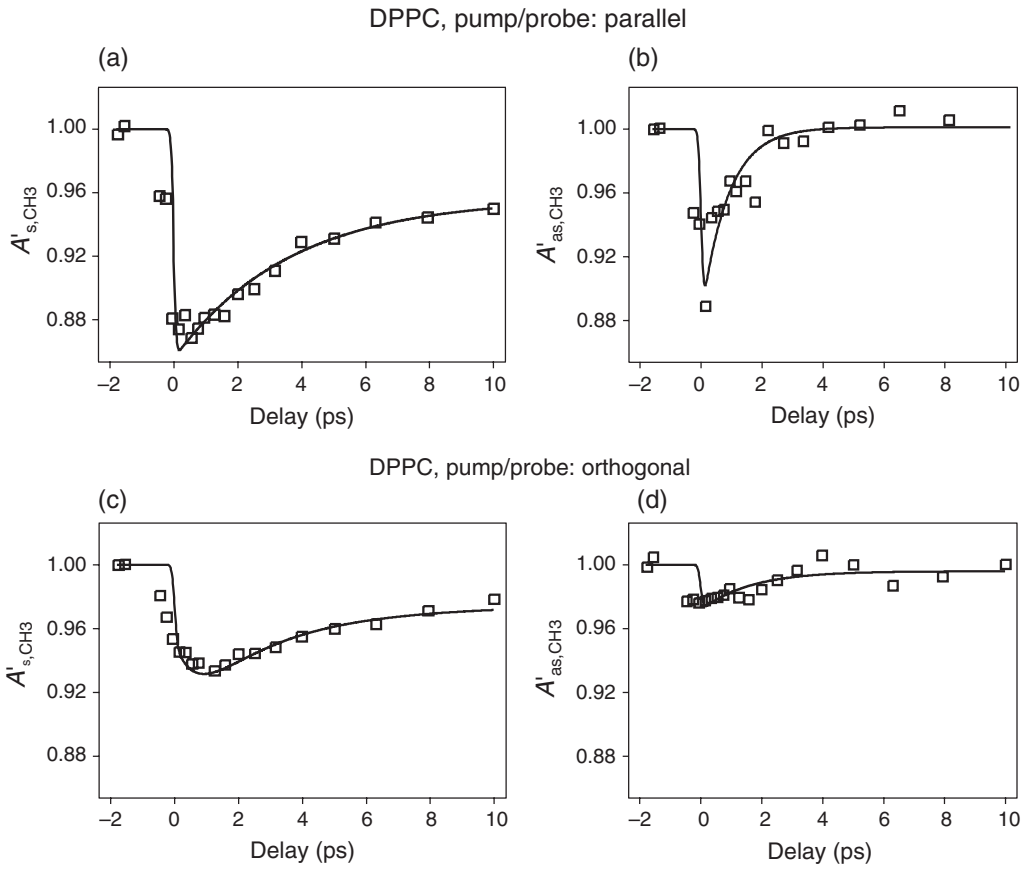

Figure 5. Time traces (open squares) are shown for DPPC for the following vibrations and polarization combinations: SSP (pump: P-polarized), $\nu_{s,CH3}$ (a); SSP (pump: P-polarized) $\nu_{as,CH3}$ (b); SSP (pump: S-polarized), $\nu_{s,CH3}$ (c); and SSP (pump: S-polarized), $\nu_{as,CH3}$ (d). The solid lines are fits to the experimental data models as detailed in section 5.

4.2.2. DOPC. To investigate whether the lipid vibrational dynamics are dependent on the lipid phase, i.e. the molecular conformation of the lipid, we also investigated the molecularly disordered DOPC lipid monolayer. The DOPC SFG spectrum (figure 3(b)) shows the CH_2 vibrations in addition to the CH_3 resonances, due to the presence of gauche defects in the alkyl chain that break the symmetry. This is due to the gel-to-liquid crystalline phase transition point of DOPC being well below room temperature (see cartoons next to the spectra in figure 3).

The results are shown in figure 6. Due to the disorder in the liquid expanded phase, both the SFG intensity and the bleach are much lower than those observed for DPPC. Furthermore, to disentangle all peaks, the VIS bandwidth is reduced at the cost of intensity. In figure 6, the time traces are shown (open squares) for $\nu_{s,CH3}$ (a), $\nu_{as,CH3}$ (b) and $\nu_{s,CH2}$ (c) for the parallel pump and probe polarizations.

Although the energy transfer process from the CH_2- to the CH_3-groups was observed in DPPC only for the perpendicular pump and probe polarizations, in the case of DOPC this process is clearly present for parallel polarizations as well. The reason is that in the case of DPPC the transition dipole moments of the CH_2 groups are largely restricted to the horizontal

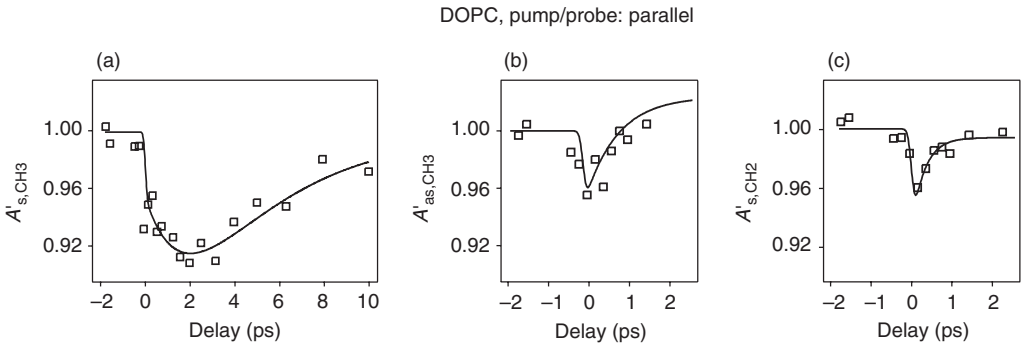

Figure 6. Time traces (open squares) are shown for DOPC for the parallel SSP (pump: P-polarized) polarization combination for $\nu_{s,CH3}$, $\nu_{as,CH3}$ and $\nu_{s,CH2}$. DOPC is in the liquid crystalline phase at room temperature. The solid lines are fits to the experimental data.

plane and cannot be excited efficiently with P-polarized pump field. In the liquid expanded phase of DOPC, many CH_2 groups have a component in the vertical plane and can be excited with the P-polarized pump field.

It is evident from figure 6 that the dynamics are remarkably similar for the two different lipids in different phases. A qualitative comparison with the results for DPPC (figure 5) reveals fast relaxation of the $\nu_{as,CH3}$ mode and slower relaxation for the $\nu_{s,CH3}$ mode in both cases. The $\nu_{s,CH2}$ symmetric CH_2 stretching mode also exhibits very fast decay.

4.2.3. Heat transfer across the monolayer. The incoherent energy transfer or heat transfer from bulk water phase across the lipid monolayer was investigated by exciting the water near the interface and monitoring the terminal CH_3 signal of DPTAP. For reference purposes, the influence of a change in temperature on the C–H region of the lipid spectrum was studied under steady-state conditions as shown in the inset in figure 7(b). For the temperature interval from 20 to 50°C, a small decrease in the overall signal is observed. Because the IR wavelength is centered further to the blue side, the spectral shape is slightly different from 3(c).

For the time-resolved studies, a two-color scheme was employed with the IR pump wavelength centered at the wing of the O–H-stretch region at $\sim$3100 cm^{-1} and the IR probe centered at the C–H-stretch region at $\sim$2900 cm^{-1}. Since the effect on the signal intensity of the CH_3 vibrations due to a temperature change is very limited, the SFG spectrum over the entire C–H stretch region (symmetric, asymmetric and Fermi-resonance) was integrated to obtain an acceptable signal-to-noise ratio. The time trace for the heat transfer process is shown in figure 7 as open squares. The change in the steady-state amplitudes due to a change in temperature is shown in figure 7(b) and was computed from the temperature-dependent spectra as shown in the inset. From the dynamical studies, a decrease of the signal level of $\sim$1.5% is found, corresponding to a change in temperature of $\sim 2^{\circ}$. To rule out any energy transfer process that does not originate from pumping the surface water molecules, the experiment was repeated with D_2O instead of H_2O. In this case, no dynamics were observed (data not shown), showing that the dynamics originate only from excitation of the water molecules, from which heat is transferred into the lipids on sub-picosecond timescales.

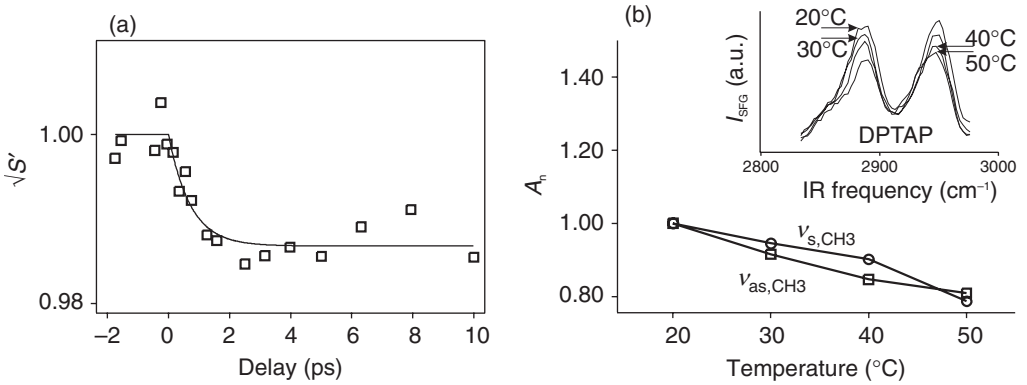

Figure 7. The time trace (open squares) is shown for heat transfer from water to DPTAP with the SSP (P-polarized pump) polarization combination (a). The contribution from CH_3 symmetric and the combination band of the antisymmetric stretch and Fermi resonance are summed together. The solid line is a fit to the experimental data. Data points between 10–100 ps (not shown) reveal that the signal remains at the value indicated by the fit at long delay times. In panel (b) the temperature dependent amplitudes of $\nu_{s,CH3}$ and $\nu_{as,CH3}$ are shown from 20 to 50°C, obtained from temperature dependent DPTAP SFG spectra, as shown in the inset.

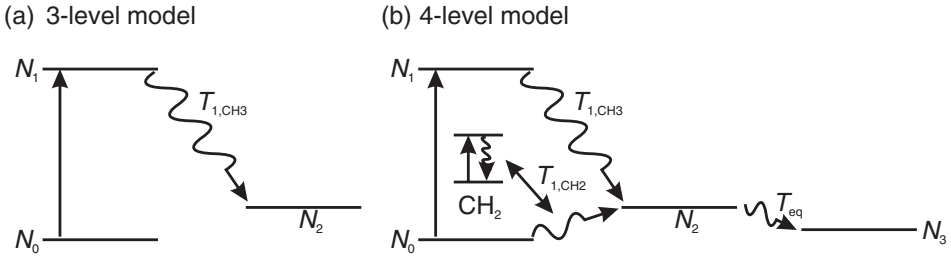

Figure 8. To describe and quantify the vibrational relaxation in lipids, 3-level (a) and 4-level (b) models are employed. In the 3-level model, after excitation the system relaxes directly to a final 'hot' ground state. In the 4-level model, both the CH_3 and the CH_2 vibrations are excited: the relaxation of the CH_3 decays to an intermediate state and the relaxation of the CH_2 results in an energy transfer from the ground state to the intermediate state. Finally, the system equilibrates to a 'hot' ground state.

4.3. Data analysis

To quantify the timescales of the vibrational relaxation and energy transfer processes from the data, we calculate the population distribution in the ground and excited states. The experimental data can be modeled according to this model and timescales can be extracted.

The simplest model to describe the features of the vibrational relaxation as observed in figures 5(a) and (b) for the SSP (P-polarized pump) polarization combination, is a three level model as shown in figure 8(a). Besides the ground state N_0 and the excited state N_1, a hot ground state N_2 is necessary to account for the slight offset of the final SFG level at long delay

times. The physical meaning of the hot ground state N_2 is that after vibrational relaxation, the temperature has increased locally. The hot ground state is populated by vibrational relaxation at a rate T_1. The differential equations that describe the time-dependent population distribution read:

$$\frac{\mathrm{d}N_0}{\mathrm{dt}} = -\sigma G(t)(N_0 - N_1), \quad \frac{\mathrm{d}N_1}{\mathrm{dt}} = \sigma G(t)(N_0 - N_1) - \frac{N_1}{T_1}, \quad \frac{\mathrm{d}N_2}{\mathrm{dt}} = \frac{N_1}{T_1}. \tag{7}$$

Here, σ is a measure of the IR cross-section, which determines the efficiency of the population transfer and $G(t)$ describes the Gaussian pulse profile of the excitation (pump) pulse. The generated SFG signal from state N_0 and N_2 is then proportional to

$$I_{\mathrm{SFG}} \propto (N_0 - N_1 + cN_2)^2, \tag{8}$$

where c accounts for a smaller/larger SFG signal from state N_2 than from the ground state N_0, caused by the heating. To fit the amplitudes for a specific vibration the square root of equation (8) is used.

It is apparent that the three level model cannot account for the observations of $\nu_{\mathrm{s,CH3}}$ in panel (c) of figure 5 for the orthogonal pump and probe polarization, as it cannot account for the delayed ingrowth of the signal. Clearly, a second process in addition to direct vibrational excitation results in a decrease of the SFG intensity. Given its strong dependence on the pump polarization, it is evident that this process must be attributed to excitation of the CH_2 modes in the lipid chain. The fact that the additional ingrowth of the signal occurs on precisely the same $\sim$1 ps timescale on which the CH_2 modes decay (see figure 6(c)) demonstrates that this energy transfer from CH_2 to CH_3 modes must be due to incoherent energy transfer, i.e. heating of the CH_3 groups due to relaxation of the CH_2 groups. The complete process can thus be modeled with the 4-level energy diagram of figure 8(b): the pump field excites the $\nu_{\mathrm{s,CH3}}$ by inducing population transfer from the ground state N_0 to the excited N_1 of this mode. At the same time the $\nu_{\mathrm{s,CH2}}$ is excited to its first vibrational level. The sub-picosecond relaxation of the CH_2 groups (figure 6(c)) results in the lipid heating up considerably, bringing the lipid and its CH_3 groups to a hot, intermediate state N_2. Relaxation of CH_3 groups themselves will also lead to a population of this state. Thermal equilibration with the water bath—i.e. heat flow out of the monolayer into the water subsystem—is reflected in the model by a transition from N_2 to the final new ground state (at elevated temperature) N_3 at a rate $1/T_{\mathrm{eq}}$. The corresponding differential equations read:

$$\begin{aligned}
\frac{\mathrm{d}N_0^{\mathrm{CH2}}}{\mathrm{dt}} &= -\sigma_{\mathrm{CH2}} G(t)(N_0^{\mathrm{CH2}} - N_1^{\mathrm{CH2}}), \quad \frac{\mathrm{d}N_1^{\mathrm{CH2}}}{\mathrm{dt}} = \sigma_{\mathrm{CH2}} G(t)(N_0^{\mathrm{CH2}} - N_1^{\mathrm{CH2}}) - \frac{N_1^{\mathrm{CH2}}}{T_{1,\mathrm{CH2}}}, \\
\frac{\mathrm{d}N_0}{\mathrm{dt}} &= -\sigma_{\mathrm{CH3}} G(t)(N_0 - N_1), \quad \frac{\mathrm{d}N_1}{\mathrm{dt}} = \sigma_{\mathrm{CH3}} G(t)(N_0 - N_1) - \frac{N_1}{T_{1,\mathrm{CH3}}}, \\
\frac{\mathrm{d}N_2}{\mathrm{dt}} &= \frac{N_1}{T_{1,\mathrm{CH3}}} + \Delta \frac{N_1^{\mathrm{CH2}}}{T_{1,\mathrm{CH2}}} - \frac{N_2}{T_{\mathrm{eq}}}, \quad \frac{\mathrm{d}N_3}{\mathrm{dt}} = \frac{N_2}{T_{\mathrm{eq}}}.
\end{aligned} \tag{9}$$

Here, σ_{CH3} and σ_{CH2} are IR cross-sections determining of the population transfers to respectively $\nu_{\mathrm{s,CH3}}$ and $\nu_{\mathrm{s,CH2}}$, and Δ is a measure for the strength of the effect of the relaxed CH_2 mode on the CH_3 mode. The signal is then given by

$$I_{\mathrm{SFG}} \propto \left(N_0 - N_1 + cN_2 + c'N_3\right)^2, \tag{10}$$

where c and c' account for the SFG signal strengths from the intermediate and final level.

Finally, for the model to describe the heat transfer from the water to the lipids (experiments shown in figure 7), we assume a single exponential process. We have previously established that vibrational relaxation of water molecules at low O–H stretch frequencies occurs very quickly (sub-50 fs) [62], so that heat is deposited quasi-instantaneously at the lipid interface. Its flow into the lipid layer is assumed to follow simple exponential behavior. Hence, due to the heating from initial temperature T_0 to final temperature T_f, the nonlinear susceptibility $\chi(t)$ evolves in time from $\chi(T_0)$ to $\chi(T_f)$ at an exponential rate $1/T_t$ as (see figure 8)

$$\chi(t) \propto (\chi(T_0) - \chi(T_f)) \exp(-t/T_t) + \chi(T_f), \tag{11}$$

with the SFG signal proportional to $\chi(t)^2$, where the superscript (2) has been omitted for clarity.

The data for DPPC in figures 5(a), (b) and (d) is fitted using the 3-level model as CH_2 excitation is minimal for the P-polarized pump pulse. The time constant for the vibrational relaxation of $\nu_{s,CH3}$ in the parallel pump and probe polarization is found to be $T_1 = 3.6 \pm 0.5$ ps. For $\nu_{as,CH3}$ the time constant is fitted globally for the parallel and orthogonal pump/probe data and is found to be $T_1 = 1.0 \pm 0.3$ ps. The data for DOPC in figure 6(b) and (c) are also fitted with the 3-level model and yields time constants of $T_1 = 0.8 \pm 0.3$ ps for the $\nu_{as,CH3}$ and $T_1 = 0.8 \pm 0.3$ ps for the $\nu_{s,CH2}$. The heat transfer rate for the H_2O-DPTAP system is modeled with equation (11) and yields a time constant of T_t=0.95 ±0.4 ps. Finally, the $\nu_{s,CH3}$ data with CH_2 energy transfer for DPPC (figure 5(c)) and DOPC (figure 6(a)) are both reproduced with the 4-level model. All time constants are fixed, as they have been determined independently in the other measurements, i.e. $T_{1,CH3} = 3.6$ ps, $T_{1,CH2} = 0.8$ ps and $T_{eq} = 0.95$ ps. For T_{eq}, it is assumed that the energy transfer from the lipid to the subphase (i.e. the equilibration process) occurs at the same rate at which the transfer from the subphase to the lipid occurs.

5. Discussion

The vibrational relaxation of the C–H stretching mode has been investigated in numerous studies in bulk liquids [63, 64]. It has been shown that the pathway of relaxation of all C–H stretching vibrations occurs via the same intermediate level and therefore the different vibrations show similar dynamics [63]. The vibrational lifetime $\tau = 3.6$ ps for $\nu_{s,CH3}$ in the terminal methyl groups of DPPC and DOPC is comparable to the bulk values. It is also similar to the $\nu_{s,CH3}$ lifetime of acetonitrile at the acetonitrile–air interface and the $\nu_{s,CH3}$ lifetime within a Cd stearate monolayer on silver [35, 65]. The lifetime $\tau = 1.2$ ps for the asymmetric $\nu_{as,CH3}$ is significantly faster than the observed lifetimes of $\nu_{s,CH3}$, indicating that unlike in bulk liquid, the vibrational pathway is distinctly different for the two modes.

The much faster relaxation of $\nu_{as,CH3}$ can be explained by strong coupling of the $\nu_{as,CH3}$ to the CH_2 vibration. For these two modes, the transition dipoles lie in the same plane, and dipole–dipole coupling is expected to play an important role. The CH_2 vibrations are highly delocalized in the all-trans chains, which may account for the faster relaxation than in bulk where the chains have more random conformations, and the CH_2 vibrations are expected to be localized. Another possible effect that may play a role in the apparent fast relaxation is the rotational motion of the terminal methyl group around the C–C bond [66]–[68]. This reorientation does not affect the $\nu_{s,CH3}$, since its transition moment is parallel to the axis of rotation. For the in-plane $\nu_{as,CH3}$ vibration, the rotational motion leads to dephasing of the $\nu_{as,CH3}$ vibration on the timescale of $T_2 = 0.8$ ps [67]. It is clear that the relatively high degree of order within the lipid alkyl chain even for the crystalline liquid DOPC facilitates vibrational relaxation and energy transfer.

Energy transfer across membranes and cooling has been studied previously in reverse micelles [13, 69]. It has been shown, using micelles of different sizes, that the cooling within the interior water, can be well described using classical thermodynamics [69]. The energy transfer across a surfactant layer can actually follow different pathways [13]. The timescale of $\tau = 0.95$ ps obtained here, is in good agreement with the value found for the energy transfer from the interior water to the polar headgroup of the surfactant in the reverse micelles [13].

To summarize, the energy flow in model lipid membranes after vibrational excitation can be described with three time constants. The $\nu_{s,CH3}$ relaxes with a time constant of $T = 3.6$ ps, comparable to findings in bulk studies. Unlike in bulk, in lipid membranes with the chains in an all-trans conformation, the $\nu_{as,CH3}$ is strongly coupled to the CH_2 vibration and shows a much faster relaxation time of $T = 0.8$ ps. The fast relaxation of the CH_2 mode is tentatively attributed to delocalization of CH_2 modes. In principle, one would expect the CH_2 relaxation to slow down for the DOPC monolayer, due to the presence of gauche defects in the alkyl chain that will reduce the delocalization of the CH_2 vibrations. Apparently, the number of gauche defects is insufficient to reduce the vibrational relaxation rates. Finally, the energy transfer between the subphase and lipid membranes or equivalently the equilibration to a hot ground state takes place on a timescale of $T_{eq} = 0.95$ ps.

6. Conclusions and outlook

We have reported the dynamics of energy flow in a biomimetic lipid monolayer using surface-specific, femtosecond time-resolved vibrational spectroscopy. We find that relaxation of C–H stretching modes occur on very short timescales, with marked variations for different modes, in contrast to observations for bulk alkanes. The technique also allows us to elucidate energy transfer times across the lipid monolayer, providing insights into the dynamics of water–membrane interactions. The successful application of this technique to the study of model membranes, as presented here, paves the way for a novel class of experiments to study biomolecular dynamics in membrane systems, including the dynamics of conformational fluctuations and transformations of specifically membrane proteins.

Acknowledgments

This work is part of the research program of the Stichting Fundamenteel Onderzoek der Materie (Foundation for Fundamental Research on Matter) with financial support from the Nederlandse Organisatie voor Wetenschappelijk Onderzoek (Netherlands Organization for the Advancement of Research). We are grateful to Anders Nilsson for his support of SY during his involvement in this work, and George Wurpel and Maria Sovago for helpful discussions and providing us with steady-state SFG spectra.

References

[1] Martin M M and Hynes J T (ed) 2004 *Femtochemistry and Femtobiology: Ultrafast Events in Molecular Science* (Elsevier: Amsterdam)

[2] Kimble M and Castleman W Jr (ed) 2006 *Femtochemistry VII: Fundamental Ultrafast Processes in Chemistry* (Amsterdam: Elsevier)

[3] Brixner T, Stenger J, Vaswani H M, Cho M, Blankenship R E and Fleming G R 2005 *Nature* **434** 625

[4] Lu H P, Xun L Y and Xie X S 1998 *Science* **282** 1877
[5] Sachs J N and Engelman D M 2006 *Annu. Rev. Biochem.* **75** 707
[6] Frauenfelder H, McMahon B H, Austin R H, Chu K and Groves J T 2001 *Proc. Natl Acad. Sci. USA* **98** 2370
[7] Wang Y H, Baskin J S, Xia T B and Zewail A H 2004 *Proc. Natl Acad. Sci. USA* **101** 18000
[8] Finkelstein I J, Ishikawa H, Kim S, Massari A M and Fayer M D 2007 *Proc. Natl Acad. Sci. USA* **104** 2637
[9] Austin R H, Xie A H, van der Meer L, Redlich B, Lindgard P A, Frauenfelder H and Fu D 2005 *Phys. Rev. Lett.* **94** 128101
[10] Lim M H, Hamm P and Hochstrasser R M 1998 *Proc. Natl Acad. Sci. USA* **95** 15315
[11] Fang C, Senes A, Cristian L, DeGrado W F and Hochstrasser R M 2006 *Proc. Natl Acad. Sci. USA* **103** 16740
[12] Douhal A and Santamaria J (ed) 2002 *Femtochemistry and Femtobiology, Ultrafast Dynamics in Molecular Science* (London: Imperial College Press)
[13] Deak J C, Pang Y S, Sechler T D, Wang Z H and Dlott D D 2004 *Science* **306** 473
[14] Volkov V V, Nuti F, Takaoka Y, Chelli R, Papini A M and Righini R 2006 *J. Am. Chem. Soc.* **128** 9466
[15] Volkov V V, Palmer D J and Righini R 2007 *J. Phys. Chem.* B **111** 1377
[16] Mukherjee P, Kass I, Arkin I and Zanni M T 2006 *Proc. Natl Acad. Sci. USA* **103** 8571
[17] Gumbart J, Wang Y, Aksimentiev A, Tajkhorshid E and Schulten K 2005 *Curr. Opin. Struct. Biol.* **15** 423
[18] Lu W Y, Kim J, Qiu W H and Zhong D P 2004 *Chem. Phys. Lett.* **388** 120
[19] Bacia K, Kim S A and Schwille P 2006 *Nat. Methods* **3** 83
[20] Borbat P P, Costa-Filho A J, Earle K A, Moscicki J K and Freed J H 2001 *Science* **291** 266
[21] Marsh D and Horvath L I 1998 *Biochim. Biophys. Acta—Rev. Biomembr.* **1376** 267
[22] Nevzorov A A and Brown M F 1997 *J. Chem. Phys.* **107** 10288
[23] McConnell H and Radhakrishnan A 2006 *Proc. Natl Acad. Sci. USA* **103** 1184
[24] Rheinstadter M C, Seydel T and Salditt T 2007 *Phys. Rev.* E **75** 011907
[25] Rheinstadter M C, Ollinger C, Fragneto G, Demmel F and Salditt T 2004 *Phys. Rev. Lett.* **93** 108107
[26] Tristram-Nagle S and Nagle J F 2004 *Chem. Phys. Lipids* **127** 3
[27] Salditt T, Li C H and Spaar A 2006 *Biochim. Biophys. Acta—Biomembr.* **1758** 1483
[28] Nagle J F and Tristram-Nagle S 2000 *Biochim. Biophys. Acta—Biomembr.* **1469** 159
[29] Kaganer V M, Mohwald H and Dutta P 1999 *Rev. Mod. Phys.* **71** 779
[30] Shen Y R 1989 *Nature* **337** 519
[31] Eisenthal K B 1996 *Chem. Rev.* **96** 1343
[32] Moad A J and Simpson G J 2004 *J. Phys. Chem.* B **108** 3548
[33] Guyot-Sionnest P, Dumas P, Chabal Y J and Higashi G S 1990 *Phys. Rev. Lett.* **64** 2156
[34] Harris A L, Rothberg L, Dubois L H, Levinos N J and Dhar L 1990 *Phys. Rev. Lett.* **64** 2086
[35] Sass M, Lettenberger M and Laubereau A 2002 *Chem. Phys. Lett.* **356** 2840
[36] Benderskii A V and Eisenthal K B 2002 *J. Phys. Chem.* A **106** 7482
[37] Nguyen K T, Shang X M and Eisenthal K B 2006 *J. Phys. Chem.* B **110** 19788
[38] McGuire J A and Shen Y R 2006 *Science* **313** 1945
[39] Smits M, Ghosh A, Sterrer M, Muller M and Bonn M 2007 *Phys. Rev. Lett.* **98** 098302
[40] Kubota J and Domen K 2007 *Anal. Bioanal. Chem.* **388** 17
[41] Lane I M, King D A and Arnolds H 2007 *J. Chem. Phys.* **126** 024707
[42] Yeagle P L 2005 *The Structure of Biological Membranes* (Washington, DC: CRC Press)
[43] Koynova R and Caffrey M 2002 *Chem. Phys. Lipids* **115** 107
[44] Fujiwara T, Ritchie K, Murakoshi H, Jacobson K and Kusumi A 2002 *J. Cell Biol.* **157** 1071
[45] Korlach J, Schwille P, Webb W W and Feigenson G W 1999 *Proc. Natl Acad. Sci. USA* **96** 8461
[46] Lagerholm B C, Weinreb G E, Jacobson K and Thompson N L 2005 *Annu. Rev. Phys. Chem.* **56** 309
[47] Conboy J C, Messmer M C and Richmond G L 1996 *J. Phys. Chem.* **100** 7617
[48] Watry M R, Tarbuck T L and Richmond G I 2003 *J. Phys. Chem.* B **107** 512
[49] Ma G and Allen H C 2006 *Langmuir* **22** 5341
[50] Chen X Y, Clarke M L, Wang J and Chen Z 2005 *Int. J. Mod. Phys.* B **19** 691

[51] Gurau M C, Castellana E T, Albertorio F, Kataoka S, Lim S M, Yang R D and Cremer P S 2003 *J. Am. Chem. Soc.* **125** 11166
[52] Hansch T W and Inguscio M (ed) 1994 *Frontiers in Laser Spectroscopy, Proceedings of the International School of Physics Enrico Fermi, Course CXX, 23 June–3 July 1992* (Amsterdam: Elsevier)
[53] van der Ham E W M, Vrehen Q H F and Eliel E R 1996 *Opt. Lett.* **21** 1448
[54] Richter L J, Petralli-Mallow T P and Stephenson J C 1998 *Opt. Lett.* **23** 1594
[55] Smits M, Sovago M, Wurpel G W H, Kim D, Muller M and Bonn M 2007 *J. Phys. Chem.* C **111** 8878
[56] Petryk M W P and Henry B R 2005 *J. Phys. Chem.* A **109** 7113
[57] Chin R P, Blase X, Shen Y R and Louie S G 1995 *Europhys. Lett.* **30** 399
[58] Yee T K and Gustafson T K 1978 *Phys. Rev.* A **18** 1597
[59] Hunt J H, Guyot-Sionnest P and Shen Y R 1987 *Chem. Phys. Lett.* **133** 189
[60] Dokter A M, Woutersen S and Bakker H J 2005 *Phys. Rev. Lett.* **94** 178301
[61] Bonn M, Hess C, Funk S, Miners J H, Persson B N J, Wolf M and Ertl G 2000 *Phys. Rev. Lett.* **84** 4653
[62] Ghosh A, Smits M, Bredenbeck J and Bonn M 2007 *J. Am. Chem. Soc.* **129** 9608
[63] Graener H and Laubereau A 1982 *Appl. Phys.* B **29** 213
[64] Deak J C, Iwaki L K and Dlott D D 1998 *Chem. Phys. Lett.* **293** 405
[65] Harris A L and Levinos N J 1989 *J. Chem. Phys.* **90** 3878
[66] Wei X and Shen Y R 2001 *Phys. Rev. Lett.* **86** 4799
[67] Sung J H and Kim D 2007 *J. Phys. Chem.* C **111** 1783
[68] Fourkas J T, Walker R A, Can S Z and Gershgoren E 2007 *J. Phys. Chem.* C **111** 8902
[69] Seifert G, Patzlaff T and Graener H 2002 *Phys. Rev. Lett.* **88** 147402